Materials Today Communications 33 (2022) 104308

Contents lists available at ScienceDirect

Materials Today Communications

journal homepage: www.elsevier.com/locate/mtcomm

Simulations of irradiation resistance and mechanical properties under irradiation of high-entropy alloy NiCoCrFe

Yan Yu, Yang Yu *

School of Physics and Optoelectronic Engineering, Nanjing University of Information Science and Technology, Nanjing 210044, Jiangsu, China

ARTICLE INFO

Keywords:
Molecular dynamics simulations
High-entropy alloy
Irradiation resistance
Tensile strength

ABSTRACT

Investigating how High-entropy alloys (HEAs) perform after high energy irradiation is significant for its industrial application. In this work, molecular dynamics simulations have been conducted to clarify the irradiation damage process of NiCoCrFe high-entropy alloy (HEA) after low energy (5 KeV), medium energy (30 KeV), and high energy (70 KeV) irradiation. Irradiation energy up to 70 KeV is used to reflect the high-energy irradiation response of HEAs. The intrinsic evolution after applying tensile stress to the irradiated system is revealed. We find that the distribution of irradiation defects in NiCoCrFe is relatively scattered. And because of atomic disordering, the lower thermal conductivity and the retarded motion of interstitial defects enable Frenkel pairs in NiCoCrFe to recombine. Thus smaller clusters and fewer dislocations are found, especially when exposed to high-energy radiation. As a result, the decline of the mechanical properties such as ultimate strength and ductility is less in NiCoCrFe than Ni when applying tensile stress to the irradiated systems. Remarkably, In NiCoCrFe, the declining rate of ultimate strength and yield strain after high energy irradiation has only a 1 % increase compared with medium energy irradiation. These results demonstrated the radiation resistance of high-entropy alloys, and reflect the stability of the mechanical properties of NiCoCrFe withstanding high-energy radiation.

1. Introduction

In the nuclear power industry, high-energy particles generated in the fusion reactor will collide with lattice atoms of the material and cause changes in the material's internal structure, leading to changes in the macroscopic thermal and mechanical properties of the material. These changes are called radiation damage. The vessel is exposed to radiation for a long time in the reactor, so choosing a suitable irradiation-resistant material has become essential in nuclear power plants [1].

High-entropy alloys (HEAs) were defined as a new type of alloy material containing five or more principal elements in approximately the same proportion [2]. But with the deepening of research, the scope of high-entropy alloys has gradually expanded, including some quaternary sub-systems of the HEAs. Due to the compositional complexity in HEAs, high-level lattice distortion and sluggish diffusion effect were produced and bring up many unique properties [3–6], such as high yield strength, high hardness, and excellent ductility and fracture toughness [7,8]. Moreover, compared with conventional alloys, HEAs have proven to possess high irradiation resistance in experiments [6,9] and simulations [10,11]. Because of these superior properties, HEA is considered a potential candidate for the first-wall material in the nuclear power industry.

The HEAs can be produced using Vacuum-arc-melting [12] or Mechanical Alloying (MA) method [13], combining different elements in nearly the same ratio into an alloy system. It is impressive that they tend to form multiphase structures containing FCC, BCC, and HCP structures. Due to the complex structure and various element combinations of high-entropy alloys, computational simulation methods are usually used for research and composition design. Among those HEAs, the Cantor alloy (CrMnFeCoNi) and Cantor-derived alloys have a surprisingly simple FCC single-phase structure [14]. Therefore, when constructing a model of the Cantor alloy, we can easily describe it as an FCC crystal in which different elements homogeneously distribute it.

In previous studies, the tensile mechanical properties of HEAs after irradiation using computational simulation methods have rarely been investigated. According to conventional metallurgical theory, some studies concentrate on evaluating how the irradiation defects affect the tensile strength of the pure zirconium and calculating the stress-strain curves of Zr with Molecular Dynamics (MD) simulations. These studies demonstrated that irradiation damage would significantly impact the

* Corresponding author.
E-mail address: yuyang@nuist.edu.cn (Y. Yu).

https://doi.org/10.1016/j.mtcomm.2022.104308
Received 11 June 2022; Received in revised form 18 August 2022; Accepted 22 August 2022
Available online 27 August 2022

static performance of materials, including yield stress decreases and elastic modulus changes [15,16]. Studying how high-entropy alloys perform after irradiation is of great significance for their industrial application, which has aroused our interest. So we investigated NiCoCrFe HEA and the conventional metal material nickel for comparison in this work. Moreover, higher radiation energy (70 KeV) than in previous studies of HEA radiation simulations was chosen so that the influences of irradiation defects would be closer to the actual conditions. Molecular dynamics have been conducted to clarify the irradiation damage process and reveal the intrinsic evolution after applying stress to the irradiated system.

2. Methods

All the molecular dynamic simulations in this paper were conducted by a large-scale atomic/molecular massively parallel simulator (LAMMPS) [17]. When setting the model of HEA, Atomsk was also used [18]. The interatomic interactions of NiCoCrFe are represented by the embedded atom method (EAM) potential [19], which features a spline to short-range ZBL potential. This potential is suitable for describing the interatomic interaction in high-energy atomic collisions in cascades. The same potential was applied for the nickel to control variables.

2.1. Radiation damage process

Firstly, two crystal models in the size of 45a × 45a × 45a (a = 3.61 Å, a is the lattice constant) with a total number of 364,500 atoms are established. Then three-dimensional periodic boundary conditions are applied, and the relaxation is performed at 300 K and NPT ensemble for 100 ps. During the simulation, the mass center of the system remains the same. When the irradiation energy is up to 30 KeV and 70 KeV, to ensure the temperature of the system remains stable and avoid the channel effect, the system is enlarged to 80a × 80a × 80a and 100a × 100a × 100a with a total number of 2,048,000 atoms and 4,000,000 atoms, respectively.

A primary knocked-on atom (PKA) far from the boundary was selected and introduced certain kinetic energy to start cascade collisions simulation. All the primary knocked-on atoms have the same velocity direction. At least three repeated experiments for each PKA energy were performed to reflect the trend of defect evolution in both materials. The relaxation lasted 25 ps in the NVE ensemble after the PKA was introduced. As the elements in HEA have different relative atomic masses, we selected only the ferrum atom in NiCoCrFe as PKA. The displacement distance per step was controlled within 0.02 Å, about 0.005 times the lattice length.

When comparing the irradiation resistance of the systems, the Winger-Seitz cell method from the software OVITO was applied to identify the irradiated interstitials and vacancies [20,21].

2.2. Tensile process

The systems relax for another 20 ps after the radiation damage process so that the defects are stabilized completely. Then a constant tensile strain along [0 0 1] direction at the rate of $2 \times 10^9/s$ is applied, and the stress along [0 1 0] and [1 0 0] directions remained zero. This process is performed at room temperature (300 K), and equilibrated in an NPT ensemble for 100 ps until the total tensile strain is up to 0.2. Stress along [0 0 1] direction was calculated every 1 ps.

Visualization software OVITO was used to analyze the simulation result [20], and Dislocation Analysis (DXA) method was taken to show the defects and dislocations in materials [22].

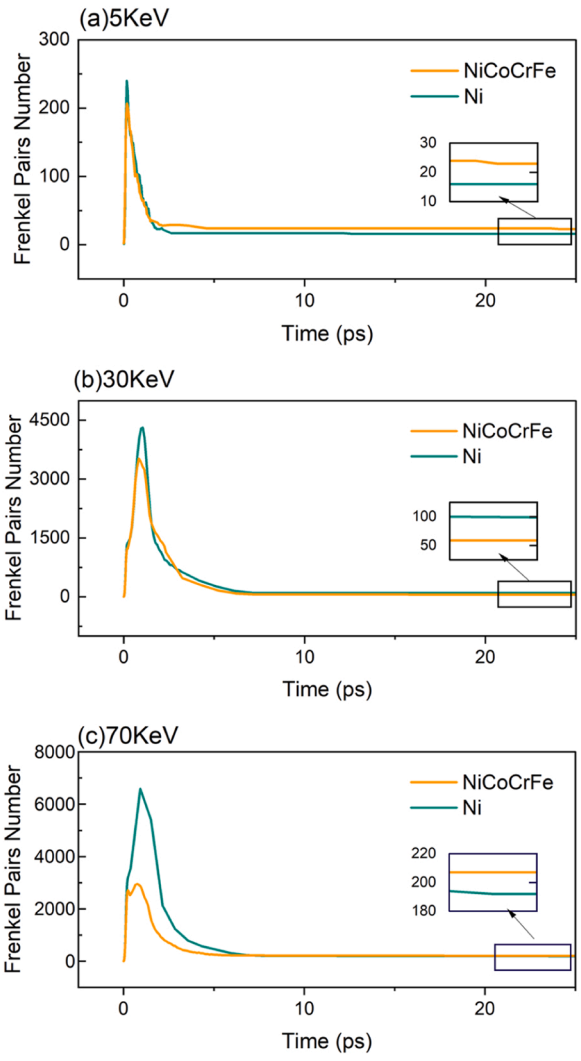

Fig. 1. The number of Frenkel pairs varies with time. (a) 5 KeV, (b) 30 KeV, (c) 70 KeV.

3. Results and discussion

3.1. Irradiation damage

3.1.1. Defect evolution

Firstly, to understand the irradiation resistance of NiCoCrFe HEA, we start with the point defects generated by radiation. The kinetic energy of PKA is 5 KeV, 30 KeV, and 70 KeV, respectively. Then the number of Frenkel pairs varies with time was counted and shown in Fig. 1.

The number of point defects increased rapidly to the peak, then recombined and disappeared gradually, remaining relatively stable at last. The maximum Frenkel pairs number (N_m) and the steady Frenkel pairs number (N_s) were introduced to describe the radiation damage. In the comprehensive view, N_s in NiCoCrFe is slightly lower than that in pure Ni. But with the increase of PKA energy, N_p in NiCoCrFe is considerably less than pure Ni.

When exposed to high-energy irradiation, the number of defects will have two peaks. The first appears shortly after the end of the ballistic council (within 0.2–0.3 ps), which is not evident. The second peak appears during the thermal spike period. Our simulations showed no obvious secondary cascade in the system irradiated at 5 KeV, but a distinct secondary peak was seen after introducing medium-energy (30 KeV) and high-energy (70 KeV) irradiation. When NiCoCrFe and pure Ni are irradiated with the same PKA energy, the number of Frenkel pairs at

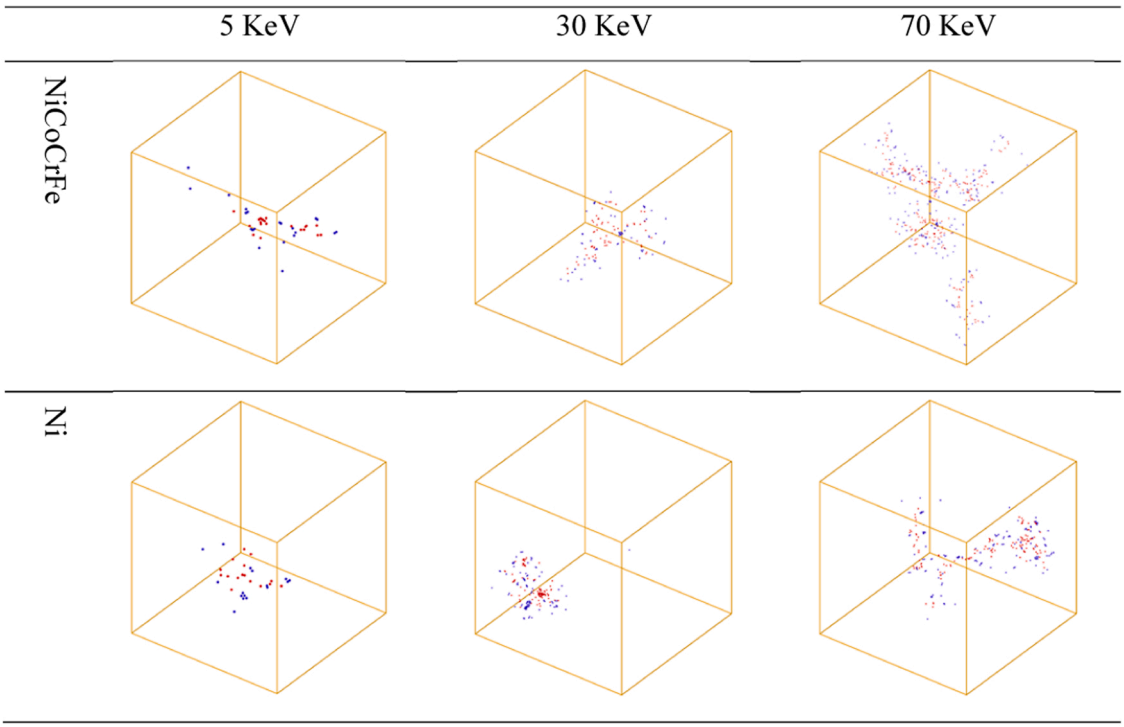

Fig. 2. Distribution of stabilized point defects (relaxed for 25 ps after irradiation) of NiCoCrFe and Ni under the radiation energy 5 KeV, 30 KeV, and 70 KeV. (For interpretation of the references to colour in this figure legend, the reader is referred to the web version of this article).

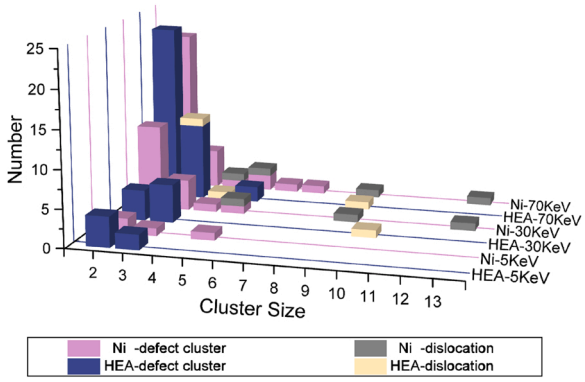

Fig. 3. Comparisons of irradiation defect cluster of NiCoCrFe (navy for the cluster, yellow for the dislocation) and Ni (pink for the cluster, grey for the dislocation) under different radiation energy. (For interpretation of the references to colour in this figure legend, the reader is referred to the web version of this article).

the first peak and N_s in NiCoCrFe are slightly less than pure Ni, but N_m is quite different.

During the thermal spike period, local high temperature leads to local melting, and huge numbers of irradiation defects are induced by the shock wave [23,24], so the influence of the energy dissipation is considerable. The experimental results reported by Zhang et al. [25] declared the influence of thermal conductivity on HEAs' irradiation resistance. The disorder-induced reduced thermal conductivity in HEAs may cause the difference in N_m [19]. Although in paper [26] they had demonstrated that the nature of the final radiation damage has little to do with the sub-cascade, this property may explain that defects in HEAs are not easy to accumulate, reflecting the ability of HEAs to resist high-energy irradiation.

There also existed simulations that proved NiCoCrFe HEA has a higher defect recombination rate than pure Ni, which have to do with the thermal spike period [27]. Furthermore, through its results, we can find that as the irradiation energy increases, the radiation tolerance difference between NiCoCrFe and Ni appears more obvious, which is shown in our simulations as well.

3.1.2. *Size and distributions of defects*

As an expression of defects distribution, the Winger-Seitz cell method was performed to recognize the stabilized point defects, and the results are shown in Fig. 2. The red dots represent vacancies, while the blue ones are interstitials.

A large number of point defects generated from the cascade will combine into defect clusters or dislocations. So, we try to count the number of defects in each cluster or dislocation to clarify the distribution of defects. And the statistical results are shown in Fig. 3. The navy and pink histograms stand for the defect cluster of HEA and Ni, respectively, and the yellow and grey histogram is the dislocation of HEA and Ni. According to the research on conventional metallic materials [16], we learned that it is mainly interstitial defects that affect the material's mechanical proper, and this phenomenon can be observed in our simulations, too. Thus, only interstitials were counted in this work.

When comparing HEA to pure Ni, the distribution of defects is relatively scattered for the HEA, and the size of defect clusters seems to be smaller. Also, the irradiation-induced dislocations in NiCoCrFe are less than pure Ni.

In line with previous studies, experiments taken by Lu et al. [9] and Mu et al. [28] show that the dislocation loop size and defect size will decrease as the compositional complexity increases, and they ascribe it to the suppressed motion of interstitial defects in complex alloys (including NiCoCrFe), which enhanced the recombination of defect pairs. Molecular dynamic simulation [29] explained that because NiCr or NiFe has higher migration barriers than pure Ni, the slow diffusion of point defects inhibits the formation of large defect clusters. Compared to those studies, our investigation also figures that the NiCoCrFe shows better irradiation resistance when the irradiation energy increases, indicating that those effects may be more pronounced when reacting to high energy.

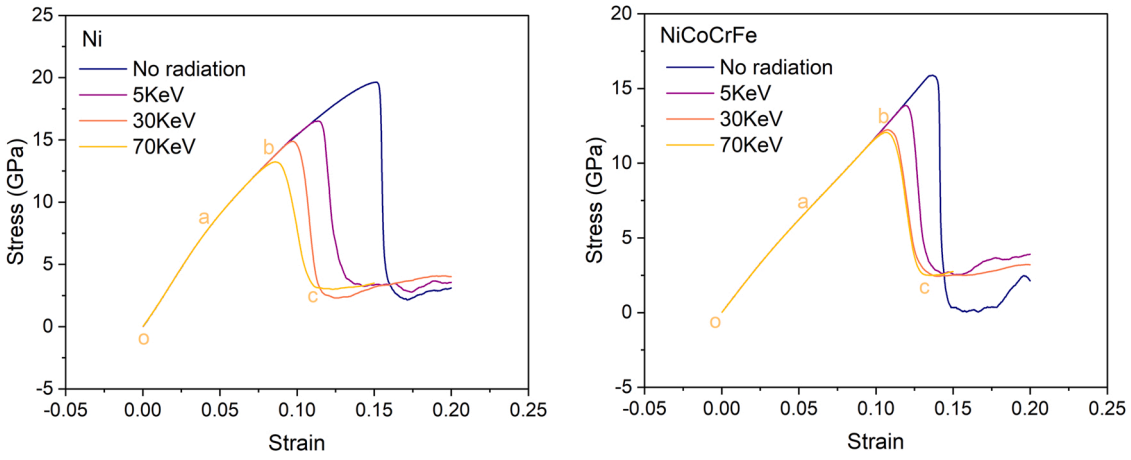

Fig. 4. Stress-strain curves of tensile tests after different energy irradiation (left: Ni, right: NiCoCrFe).

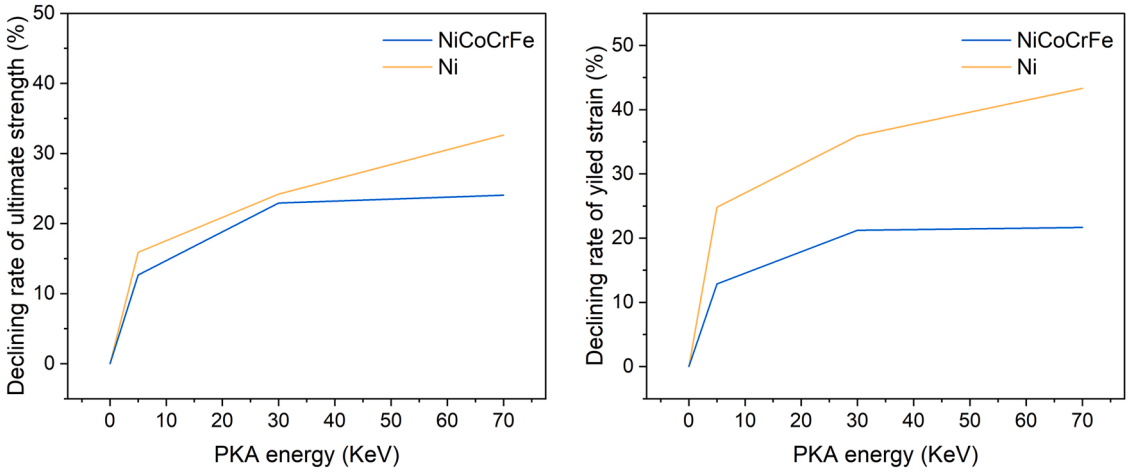

Fig. 5. The declining rate of ultimate strength (left) and yield strain (right).

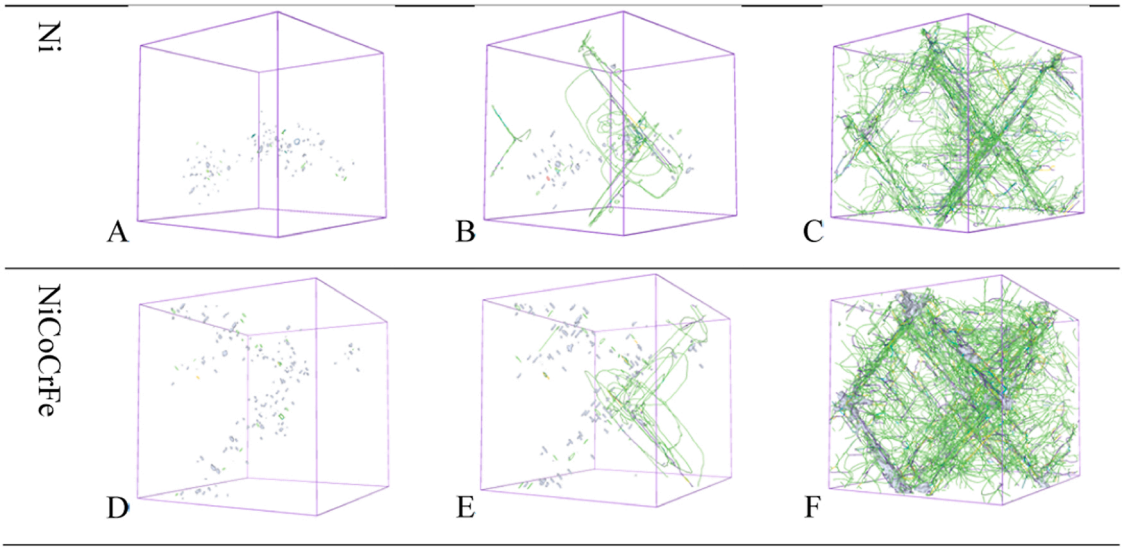

Fig. 6. Snapshot of the microstructure of 3 crucial points after 70KeV irradiation. A, B, and C are taken from the Ni model, corresponding to points a, b, and c in Fig. 4(a), A: strain = 0.044, B: strain = 0.086, C: strain = 0.106. And D, E, F are taken from NiCoCrFe model, corresponding to points a, b, and c in Fig. 4(b), D: strain = 0.056, E: strain = 0.106, F: strain = 0.128. (For interpretation of the references to colour in this figure legend, the reader is referred to the web version of this article.)

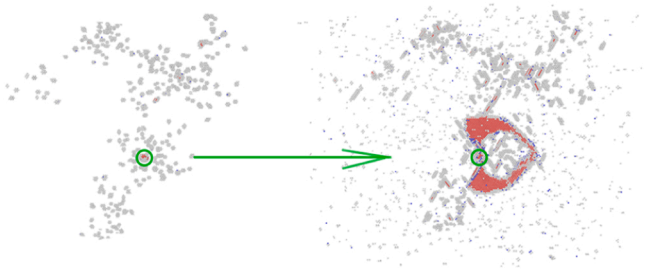

Fig. 7. Snapshot of the microstructure of NiCoCrFe after 70KeV irradiation. (Left: strain = 0, right: strain = 0.096). (For interpretation of the references to colour in this figure legend, the reader is referred to the web version of this article.)

3.2. Mechanical properties after irradiation

3.2.1. Tensile stress-strain curve

Irradiation-induced defects have a complex interaction with dislocations when tensile stress is applied, which will change the material's mechanical properties. Tensile simulation is carried out to understand what would happen to the defects during deformation and explore how HEAs behave in terms of radiation hardening and embrittlement. Fig. 4 shows the stress-strain curves of the materials after irradiation.

The stress-strain curves have no significant difference before yield, but the yield point and yield strength obviously decrease with the irradiation energy increase. In order to reflect the trend clearly, the declining rate of ultimate strength and yield strain is shown in Fig. 5.

The results indicate that NiCoCrFe has better plasticity naturally, and the mechanical properties after irradiation changed smaller, such as ultimate strength and ductility, especially under high-energy irradiation.

These outstanding mechanical properties of the Cantor alloy are consistent with what has been found previously. Fabio et al. [30] reviewed the relevant experiments and probable causes. They also suggested that the variants of Cantor alloy, including NiCoCrFe, show an even higher ultimate strength and better ductility than other HEAs and traditional alloys. Furthermore, Cao et al. [31] revealed the incipient plasticity behaviors of CrCoNi using Density Functional (DFT) Methods, and investigated the impact of chemical inhomogeneity on special defect structure in CrCoNi.

3.2.2. Intrinsic evolution after applying tensile stress

Three crucial points a, b, and c (after 70 KeV radiation) in Fig. 4 were chosen to see how radiation affected the tensile mechanical properties. And the DXA method was applied to detect the microstructure of those models. Fig. 6 shows the results. Green, yellow, blue, and purple lines represent Shockley dislocations, Stair-rod dislocations, Perfect dislocation loop, and some unrecognized dislocations. The dark grey meshes represent defect meshes. All atoms have been hidden for ease of observation.

In section 'oa', as the strain increases continuously, the size of irradiation defects remained almost unchanged, and no new dislocations appeared. While in section 'ab', when the shear stress reaches the critical value, dislocations start to slip along <112> direction until it covers the entire material. According to the dislocation theory of plastic deformation, strain rate $\dot{\varepsilon} = b\rho v$ (b is a constant, ρ is mobile dislocation density, and v is dislocation velocity). Because of low dislocation density, high shear stress should be applied to accelerate those dislocations until the next stage. Yield occurs after point b. At this point, dislocations multiply rapidly, and hence stress decreases sharply to make sure the strain rate maintains constant. And until point c, the rate of dislocation multiply slows down because of the high density of dislocation, dislocations slipping or deforming for a long time during plastic deformation.

In contrast to unirradiated material, the irradiation-generated defects will serve as nucleation sites for dislocations. Dislocation nucleation is observed by Common Neighbor Analysis (CNA). In Fig. 7 is the result, red atoms are an HCP structure, blue atoms have a BCC structure, and white atoms are other structures. All FCC structure atoms are hidden. Those atoms constitute the slip plane. We can indicate from the result that the large defect or dislocation acts as the primary nucleation site for dislocations.

After 5 KeV irradiation, there are no irradiation-induced dislocations. Large defect clusters transform into dislocations gradually with the increase of strain and increase continuously until the plastic deformation begins. After high-energy irradiation, the dislocations generated by the radiation will increase directly with the tensile strain added. Therefore, as the irradiation energy increases, the size of defect clusters or dislocations in the material increases, then the formation and growth of dislocations will be more manageable after the tensile stress is loaded, which gives rise to a yield strength decrease.

Given the conclusion in Section 3.1, we suggest that irradiation defects in high-entropy alloys are harder to gather into large defect clusters or dislocations than in pure nickel. The special defect structure induced by the lattice distortion effect may also account [31]. We speculate that this property enables high-entropy alloys to maintain high yield strength after high-energy irradiation.

4. Conclusion

When comparing HEA to pure Ni, the distribution of irradiation defects is relatively scattered for the HEA, the size of defect clusters is smaller, and dislocations are less. This phenomenon is particularly noticeable when exposed to high-energy radiation. That is because the severe lattice distortion caused by the special composition and lattice structure of high-entropy alloy increases the formation energy of vacancies, thereby inhibiting the nucleation and growth of matrix defects such as voids and dislocation loops, resulting in the smaller size of defects. It results in the radiation resistance of high-entropy alloys.

Remarkably, differences between stress-strain curves of NiCoCrFe after high energy irradiation and medium energy are very slight, which reflects the mechanical properties stability of NiCoCrFe withstanding high-energy radiation. And we indicate that HEAs' mechanical properties are not easily affected by irradiation could be attributed to the properties of its irradiation-induced defects.

In the actual materials, on the contrary, the irradiation-generated defects may hinder the movement of original defects, or interact with the grain boundaries, thereby causing radiation hardening. Moreover, limited by the time scale of molecular dynamics, the strain rate is much higher than the reality, affecting the mechanical properties of materials [32], so the yield strength produced by simulation might be inaccurate. However, through the intrinsic structure of the crystal model, we can see the stability of mechanical properties in HEAs after irradiation and the excellent radiation resistance of it indeed. Furthermore, By studying the mechanism of tensile deformation for structural design, Zhang et al. [33] proposed the possibility of increasing the strength and ductility simultaneously, and Wei et al. [34] found that building defects by freezing pre-strain also have the same effect, reflecting that understanding the defect properties and mechanical properties of high-entropy alloys is essential.

CRediT authorship contribution statement

Yan Yu: Conceptualization, Methodology, Software, Investigation, Formal analysis, Writing – original draft. **Yang Yu:** Conceptualization, Funding acquisition, Resources, Supervision, Writing – review & editing.

Declaration of Competing Interest

The authors declare that they have no known competing financial interests or personal relationships that could have appeared to influence

the work reported in this paper.

Data Availability

Data will be made available on request.

Acknowledgement

The authors acknowledge the financial support from the National Natural Science Foundation of China (Grant No. 11704194). The numerical calculations in this paper have been done on the supercomputing system in the Supercomputing Center of Nanjing University of Information Science & Technology.

References

[1] S.J. Zinkle, G.S. Was, Materials challenges in nuclear energy, Acta Mater. 61 (3) (2013) 735–758, https://doi.org/10.1016/j.actamat.2012.11.004.
[2] J.W. Yeh, S.K. Chen, S.J. Lin, J.Y. Gan, T.S. Chin, T.T. Shun, C.H. Tsau, S.Y. Chang, Nanostructured high-entropy alloys with multiple principal elements: novel alloy design concepts and outcomes, Adv. Eng. Mater. 6 (5) (2004) 299–303, https://doi.org/10.1002/adem.200300567.
[3] L. Qian, H. Bao, R. Li, Q. Peng, Atomistic insights of a chemical complexity effect on the irradiation resistance of high entropy alloys, Mater. Adv. 3 (3) (2022) 1680–1686, https://doi.org/10.1039/d1ma01184g.
[4] K.Y. Tsai, M.H. Tsai, J.W. Yeh, Sluggish diffusion in Co–Cr–Fe–Mn–Ni high-entropy alloys, Acta Mater. 61 (13) (2013) 4887–4897, https://doi.org/10.1016/j.actamat.2013.04.058.
[5] K. Sugita, R. Ogawa, M. Mizuno, H. Araki, A. Yabuuchi, Vacancy migration energies in CrMnFeCoNi, CrFeCoNi, and CrFeNi alloys and their effect on atomic diffusion, Scr. Mater. 208 (2022), 114339, https://doi.org/10.1016/j.scriptamat.2021.114339.
[6] T. Nagase, P.D. Rack, J.H. Noh, T. Egami, In-situ TEM observation of structural changes in nano-crystalline CoCrCuFeNi multicomponent high-entropy alloy (HEA) under fast electron irradiation by high voltage electron microscopy (HVEM, Intermetallics 59 (2015) 32–42, https://doi.org/10.1016/j.intermet.2014.12.007.
[7] B. Gludovatz, A. Hohenwarter, D. Catoor, E.H. Chang, E.P. George, R.O. Ritchie, A fracture-resistant high-entropy alloy for cryogenic applications, Science 345 (6201) (2014) 1153–1158, https://doi.org/10.1126/science.1254581.
[8] J.Y. He, H. Wang, H.L. Huang, X.D. Xu, M.W. Chen, Y. Wu, X.J. Liu, T.G. Nieh, K. An, Z.P. Lu, A precipitation-hardened high-entropy alloy with outstanding tensile properties, Acta Mater. 102 (2016) 187–196, https://doi.org/10.1016/j.actamat.2015.08.076.
[9] C. Lu, T. Yang, K. Jin, N. Gao, P. Xiu, Y. Zhang, F. Gao, H. Bei, W.J. Weber, K. Sun, Y. Dong, L. Wang, Radiation-induced segregation on defect clusters in single-phase concentrated solid-solution alloys, Acta Mater. 127 (2017) 98–107, https://doi.org/10.1016/j.actamat.2017.01.019.
[10] H.S. Do, B.J. Lee, Origin of radiation resistance in multi-principal element alloys, Sci. Rep. 8 (1) (2018) 16015, https://doi.org/10.1038/s41598-018-34486-5.
[11] Y. Li, R. Li, Q. Peng, S. Ogata, Reduction of dislocation, mean free path, and migration barriers using high entropy alloy: insights from the atomistic study of irradiation damage of CoNiCrFeMn, Nanotechnology 31 (42) (2020), 425701, https://doi.org/10.1088/1361-6528/ab9cf5.
[12] K. Tseng, Y. Yang, C. Juan, T. Chin, C. Tsai, J. Yeh, A light-weight high-entropy alloy Al20Be20Fe10Si15Ti35, Sci. China Technol. Sci. 61 (2) (2018) 184–188, https://doi.org/10.1007/s11431-017-9073-0.
[13] W. Ji, Z. Fu, W. Wang, H. Wang, J. Zhang, Y. Wang, F. Zhang, Mechanical alloying synthesis and spark plasma sintering consolidation of CoCrFeNiAl high-entropy alloy, J. Alloy. Compd. 589 (2014) 61–66, https://doi.org/10.1016/j.jallcom.2013.11.146.
[14] B. Cantor, I.T.H. Chang, P. Knight, A.J.B. Vincent, Microstructural development in equiatomic multicomponent alloys, Mater. Sci. Eng.: A 375–377 (2004) 213–218, https://doi.org/10.1016/j.msea.2003.10.257.
[15] X.J. Long, B. Li, L. Wang, J.Y. Huang, J. Zhu, S.N. Luo, Shock response of Cu/graphene nanolayered composites, Carbon 103 (2016) 457–463, https://doi.org/10.1016/j.carbon.2016.03.039.
[16] Y. Li, H. Chen, Y. Chen, Y. Wang, L. Shao, W. Xiao, Point defect effects on tensile strength of α−zirconium studied by molecular dynamics simulations, Nucl. Mater. Energy 20 (2019), https://doi.org/10.1016/j.nme.2019.100683.
[17] S. Plimpton, Fast parallel algorithms for short-range molecular dynamics, J. Comput. Phys. 117 (1) (1995) 1–19, https://doi.org/10.1006/jcph.1995.1039.
[18] P. Hirel, Atomsk: a tool for manipulating and converting atomic data files, Comput. Phys. Commun. 197 (2015) 212–219, https://doi.org/10.1016/j.cpc.2015.07.012.
[19] O.R. Deluigi, R.C. Pasianot, F.J. Valencia, A. Caro, D. Farkas, E.M. Bringa, Simulations of primary damage in a high entropy alloy: probing enhanced radiation resistance, Acta Mater. 213 (2021), https://doi.org/10.1016/j.actamat.2021.116951.
[20] A. Stukowski, Visualization and analysis of atomistic simulation data with OVITO–the Open Visualization Tool, Model. Simul. Mater. Sci. Eng. 18 (1) (2009), 015012, https://doi.org/10.1088/0965-0393/18/1/015012.
[21] N. Stefanou, H. Akai, R. Zeller, An efficient numerical method to calculate shape truncation functions for Wigner-Seitz atomic polyhedra, Comput. Phys. Commun. 60 (2) (1990) 231–238, https://doi.org/10.1016/0010-4655(90)90009-P.
[22] A. Stukowski, V.V. Bulatov, A. Arsenlis, Automated identification and indexing of dislocations in crystal interfaces, Model. Simul. Mater. Sci. Eng. 20 (8) (2012), 085007, https://doi.org/10.1088/0965-0393/20/8/085007.
[23] E. Zarkadoula, S.L. Daraszewicz, D.M. Duffy, M.A. Seaton, I.T. Todorov, K. Nordlund, M.T. Dove, K. Trachenko, The nature of high-energy radiation damage in iron, J. Phys. Condens Matter 25 (12) (2013), 125402, https://doi.org/10.1088/0953-8984/25/12/125402.
[24] G.S. WAS, Fundamentals of Radiation Materials Science: Metals and Alloys, Springer New York, 2016. ⟨https://books.google.com.hk/books?id=yDGmDAAAQBAJ⟩.
[25] Y. Zhang, K. Jin, H. Xue, C. Lu, R.J. Olsen, L.K. Beland, M.W. Ullah, S. Zhao, H. Bei, D.S. Aidhy, G.D. Samolyuk, L. Wang, M. Caro, A. Caro, G.M. Stocks, B.C. Larson, I. M. Robertson, A.A. Correa, W.J. Weber, Influence of chemical disorder on energy dissipation and defect evolution in advanced alloys, J. Mater. Res. 31 (16) (2016) 2363–2375, https://doi.org/10.1557/jmr.2016.269.
[26] A.F. Calder, D.J. Bacon, A.V. Barashev, Y.N. Osetsky, On the origin of large interstitial clusters in displacement cascades, Philos. Mag. 90 (7–8) (2010) 863–884, https://doi.org/10.1080/14786430903117141.
[27] Y. Lin, T. Yang, L. Lang, C. Shan, H. Deng, W. Hu, F. Gao, Enhanced radiation tolerance of the Ni-Co-Cr-Fe high-entropy alloy as revealed from primary damage, Acta Mater. 196 (2020) 133–143, https://doi.org/10.1016/j.actamat.2020.06.027.
[28] X. Wang, C.M. Barr, K. Jin, H. Bei, K. Hattar, W.J. Weber, Y. Zhang, K.L. More, Defect evolution in Ni and NiCoCr by in situ 2.8 MeV Au irradiation, J. Nucl. Mater. 523 (2019) 502–509, https://doi.org/10.1016/j.jnucmat.2019.05.026.
[29] D.S. Aidhy, C. Lu, K. Jin, H. Bei, Y. Zhang, L. Wang, W.J. Weber, Point defect evolution in Ni, NiFe and NiCr alloys from atomistic simulations and irradiation experiments, Acta Mater. 99 (2015) 69–76, https://doi.org/10.1016/j.actamat.2015.08.007.
[30] F.D.C. Garcia Filho, R.O. Ritchie, M.A. Meyers, S.N. Monteiro, Cantor-derived medium-entropy alloys: bridging the gap between traditional metallic and high-entropy alloys, J. Mater. Res. Technol. -JmrT 17 (2022) 1868–1895, https://doi.org/10.1016/j.jmrt.2022.01.118.
[31] C. Fu-Hua, W. Yun-Jiang, D. Lan-Hong, Novel atomic-scale mechanism of incipient plasticity in a chemically complex CrCoNi medium-entropy alloy associated with inhomogeneity in local chemical environment, Acta Mater. 194 (2020) 283–294, https://doi.org/10.1016/j.actamat.2020.05.042.
[32] T.J. Gao, D. Zhao, T.W. Zhang, T. Jin, S.G. Ma, Z.H. Wang, Strain-rate-sensitive mechanical response, twinning, and texture features of NiCoCrFe high-entropy alloy: experiments, multi-level crystal plasticity and artificial neural networks modeling, J. Alloy. Compd. 845 (2020), https://doi.org/10.1016/j.jallcom.2020.155911.
[33] Z. Zhang, Z. Jiang, Y. Xie, S.L.I. Chan, J. Liang, J. Wang, Multiple deformation mechanisms induced by pre-twinning in CoCrFeNi high entropy alloy, Scr. Mater. 207 (2022), 114266, https://doi.org/10.1016/j.scriptamat.2021.114266.
[34] D. Wei, W. Gong, L. Wang, B. Tang, T. Kawasaki, S. Harjo, H. Kato, Strengthening of high-entropy alloys via modulation of cryo-pre-straining-induced defects, J. Mater. Sci. Technol. 129 (2022) 251–260, https://doi.org/10.1016/j.jmst.2022.04.055.